Article:
Musonda, E and Hunter, IC (2015) Microwave bandpass filters using re-entrant resonators. IEEE Transactions on Microwave Theory and Techniques (99). 1 - 11. ISSN 0018-9480

https://doi.org/10.1109/TMTT.2015.2389216

Microwave Bandpass Filters Using Re-entrant Resonators

Evaristo Musonda, Student Member, IEEE, Ian C. Hunter, Fellow, IEEE

Abstract — Design techniques for microwave bandpass filters using re-entrant resonators are presented. The key feature is that each re-entrant resonator in the filter generates a passband resonance and a finite frequency transmission zero, above the passband. Thus an N^{th} degree filter can have N finite frequency transmission zeros with a simple physical realization. A physically symmetrical 5 pole re-entrant bandpass filter prototype with 5 transmission zeros above the passband was designed and fabricated. Measured results showed good correspondence with theories.

Index Terms—In-line, Pseudo-elliptic filters, Re-entrant Resonator, Transmission Zeros

I. Introduction

Finite transmission zeros are routinely used to increase the selectivity of bandpass filters. Currently, there are two ways in which transmission zeroes are physically realized. The first one is through multipaths created within the filter structure which produces destructive interference at some desired frequencies called transmission zero frequencies. This is normally achieved by means of cross-coupling between non-adjacent nodes or resonators in the filter structure. The second way involves the creation of the transmission zero generating elements which are then cascaded together to form higher order networks or mixed with other elements. These techniques are well explained in [1]. However, these methods often lead to bulky filters due to high number of elements required and sometimes inconvenient topologies.

In this paper, a re-entrant resonator is used to create a bandpass resonance with an integrated finite frequency transmission zero. The concept of the re-entrant line was first introduced by Cohn in the design of couplers [2] and similar configurations were further applied in [3] for the design of wide bandpass and bandstop filters. The re-entrant cross section has also been used in [4] where the dual resonance and finite frequency transmission zero produced by a single resonator was exploited for dual bandpass applications. In this paper, the re-entrant line is used in the design of small percentage bandwidth bandpass filters, particularly with transmission zeros above the passband. Transmission zeros below the passband are also theoretically possible using this approach but impractical to realize in real systems. The proposed design offer a simple and easy implementation for pseudo elliptic filters where a higher level of attenuation is required on the high side of the passband than can be provided by conventional coaxial filters. This type of filter is useful for interference rejection in cellular base stations.

The concept of a re-entrant line resonator is developed in section II to generate bandpass resonators with integrated transmission zeros thus realizing finite frequency transmission zeros without the need for complicated cross couplings. In section III, development of the design technique for bandpass filters with transmission zeros above the passband is presented. Comparisons of the re-entrant resonator to the coaxial resonator and their merits in terms of size, loss and stopband responses are also discussed. Some design examples are given in section IV and a prototype re-entrant bandpass filter was built and laboratory tested.

II. Re-entrant Resonators

The basic concept of a re-entrant transmission line is that it is a form of triaxial transmission line with three concentric conductors one of which is grounded. Fig. 1 shows an example of an air filled re-entrant resonator. Because the inner conductor has zero admittance to ground, a re-entrant transmission line makes for practical and convenient

Manuscript submitted June 22, 2014. This work was supported in part by the Beit Trust, University of Leeds, RS Microwave Inc, Radio Design and Royal Academy of Engineering.

E. Musonda and I. C. Hunter are with the Institute of Microwave and Photonics, School of Electronic and Electrical Engineering, University of Leeds, LS2 9JT Leeds, UK.

realization as a microwave filter element. In fact this unique property alone makes the re-entrant line very useful as opposed to conventional two conductor transmission lines.

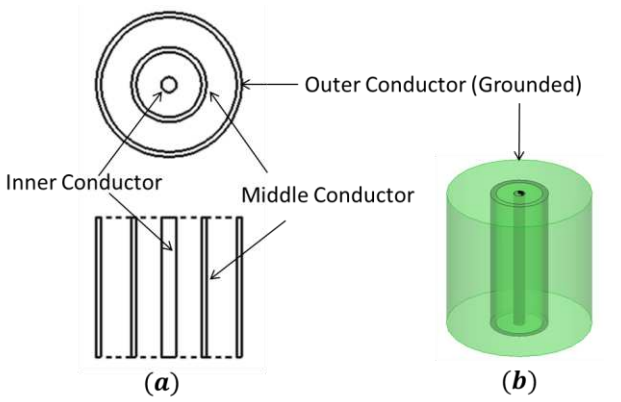

Fig. 1. A physical re-entrant transmission line: (a) top and cross section view (b) isometric view

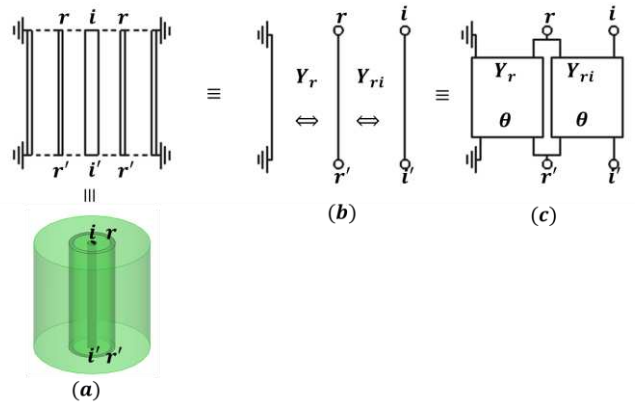

Fig. 2. A re-entrant line equivalent circuit (a) Physical transmission line (b) Graph representation (c) two series-connected transmission lines

Although, the conductors used in Fig. 1 are of cylindrical profile, other profiles such as square or rectangular coaxial may be employed where convenient. Furthermore, Fig. 1 also shows that a basic re-entrant transmission line is a four port transmission line. It is also readily seen from Fig. 1 that the equivalent circuit for the re-entrant line is two series connected transmission line networks of commensurate length (θ) as depicted in Fig. 2. Here Y_r is the admittance to ground of the middle conductor, Y_{ri} is the admittance between the middle conductor and the inner center conductor and r indicates r^{th} resonator in the filter. This equivalent circuit may be used to derive useful filtering elements by appropriately terminating two of the four ports in either short or open circuits. The choice of the termination depends on the physical realisability and required transmission characteristics.

A more useful and convenient equivalent circuit is obtained from Sato's two-wire equivalent circuit of coupled-lines [5] consisting of short circuited series stubs and transmission lines as depicted in Fig. 3. The four port numbers in [5] are replaced by variables (i.e. r, i, r' and i' as in Fig. 2). In this case, the only condition imposed on the inner conductor is that it has no admittance to ground i.e. $Y_{ii} = Y_{ri}$.

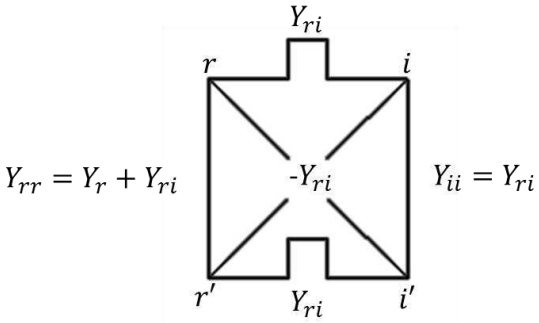

Fig. 3. Graph representation of the equivalent circuit of re-entrant line using Sato's equivalent circuit of two coupled lines

A. Re-entrant Resonator producing a transmission zero above the passband

To realize a transmission zero above the passband, two convenient re-entrant structures may be used. For case 1, the two ports on one end of the re-entrant line in Fig. 3 i.e. port r' and i', are short-circuited to the ground yielding the equivalent circuit as shown in Fig. 4(a) consisting of short-circuited stubs. This can be verified by inspection of the equivalent circuit shown in Fig. 2(c). Resonance is achieved by capacitively loading port i as shown in Fig. 4(b) and Fig. 5.

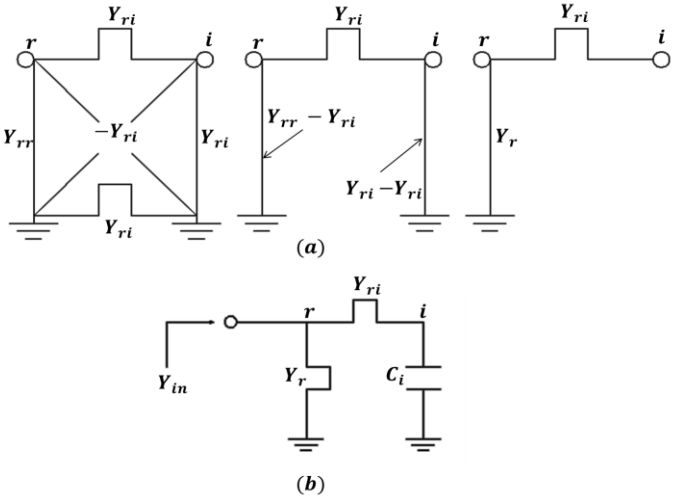

Fig. 4. Case 1 - Re-entrant resonator realizing a transmission zero above the passband (a) derivation of the equivalent circuit (b) resonance circuit.

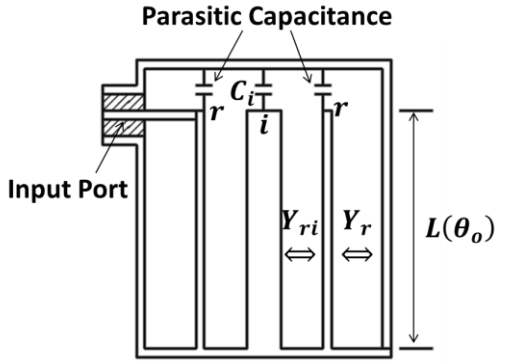

Fig. 5. Cross section of a physical realization of circuit of Fig. 4 (b)

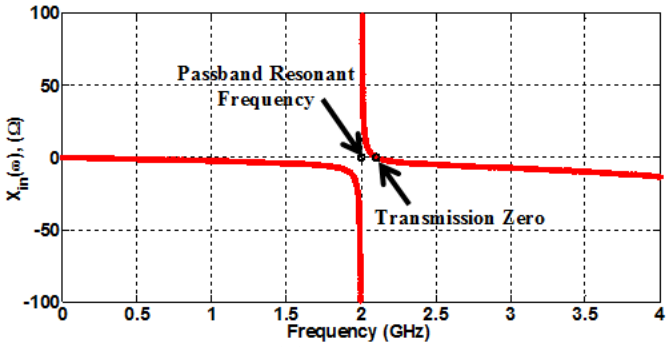

Fig. 6. Reactance function $X_{in}(\omega)$ plot corresponding to circuit of Fig. 4 (b)

The input impedance of circuit of Fig. 4(b) may be computed as

$$Z_{in}(j\omega) = j\frac{Z_r \tan(a\omega)\,(\omega C_i Z_{ri}\tan(a\omega) - 1)}{1 - \omega C_i (Z_r + Z_{ri})\tan(a\omega)} \tag{1}$$

where

$$a = \frac{\theta_o}{\omega_o} \tag{2}$$

and

$$C_i = \frac{1}{\omega_z Z_{ri}\, tan(a\omega_z)}$$

$$Z_r = Z_{ri}\left(\frac{\omega_o\, tan(a\omega_o)}{\omega_z\, tan(a\omega_z)} - 1\right). \tag{3}$$

Where, $\omega_o = 2\pi f_o$, $\omega_z = 2\pi f_z$, and θ_o are the center frequency, the position of the transmission zero frequency and the electrical length at the center frequency respectively. Circuit element values are obtained for example if $f_o = 2\,GHz$, $f_z = 2.2\,GHz$, $\theta_o = \pi/6\ rad$, and $Z_{ri} = 77\,\Omega$, then using (2) - (3), $C_i = 1.45\,pF$ and $Z_r = 18.27\,\Omega$. Plot of a reactance $X_{in}(\omega)$ of $Z_{in}(j\omega)$ against frequency is shown in Fig. 6. The presence of the parasitic capacitance in Fig. 5 results in the second passband very close to the first passband.

Although case 1 is the easiest form of realization, it does present a challenge in the filter to control the lumped capacitance at port i as well as the shortening of the open-circuit end of port r (parasitic capacitance). This may easily be solved in case 2 by short-circuiting the alternate ends of the inner and middle conductor of Fig. 2 i.e. port r' and i. The equivalent circuit for case 2 is found from the two-wire admittance matrix for coupled lines as [6],

$$\begin{bmatrix} I_r \\ I_i \\ I_{r'} \\ I_{i'} \end{bmatrix} = \frac{1}{t}\begin{bmatrix} Y_{rr} & -Y_{ri} & Y_{rr}' & -Y_{ri}' \\ -Y_{ir} & Y_{ii} & -Y_{ir}' & Y_{ii}' \\ Y_{rr}' & -Y_{ri}' & Y_{rr} & -Y_{ri} \\ -Y_{ir}' & Y_{ii}' & -Y_{ir} & Y_{ii} \end{bmatrix}\begin{bmatrix} V_r \\ V_i \\ V_{r'} \\ V_{i'} \end{bmatrix}, \tag{4}$$

where,

$Y'_{nm} = -\left(\sqrt{1-t^2}\right)Y_{nm}$, n and m are indices as in (4) (5)

$t = jtanh(ap)$, p is the complex frequency variable, and I and V are port current and voltage. Now, for case 2 port $r'$and i are short-circuited to ground so that $V_i = V_{r'} = 0$ in (4). Thus (4) may be re-written for a two-port as

$$\begin{bmatrix} I_r \\ I_{i'} \end{bmatrix} = \begin{bmatrix} \dfrac{Y_r + Y_{ri}}{t} & \dfrac{\left(\sqrt{1-t^2}\right)Y_{ri}}{t} \\ \dfrac{\left(\sqrt{1-t^2}\right)Y_{ri}}{t} & \dfrac{Y_{ri}}{t} \end{bmatrix}\begin{bmatrix} V_r \\ V_{i'} \end{bmatrix}. \tag{6}$$

Where the substitution

$$\begin{aligned} Y_{rr} &= Y_r + Y_{ri} \\ Y_{ii} &= Y_{ri} \\ Y_{ri} &= Y_{ir} \end{aligned} \tag{7}$$

was made to arrive at (6). The two-port admittance matrix between port r and i' from (6) is

$$[Y] = \begin{bmatrix} \dfrac{Y_r + Y_{ri}}{t} & \dfrac{\left(\sqrt{1-t^2}\right)Y_{ri}}{t} \\ \dfrac{\left(\sqrt{1-t^2}\right)Y_{ri}}{t} & \dfrac{Y_{ri}}{t} \end{bmatrix}. \tag{8}$$

This may be converted to ABCD matrix as

$$[ABCD] = \frac{1}{\sqrt{1-t^2}}\begin{bmatrix} -1 & -\dfrac{t}{Y_{ri}} \\ -\left(\dfrac{Y_r}{t} + Y_{ri}t\right) & -\left(\dfrac{Y_r}{Y_{ri}} + 1\right) \end{bmatrix}. \tag{9}$$

Which may further be decomposed into

$$[ABCD] = \begin{bmatrix} 1 & 0 \\ \dfrac{Y_r}{t} & 1 \end{bmatrix}\begin{bmatrix} -1 & 0 \\ 0 & -1 \end{bmatrix}\frac{1}{\sqrt{1-t^2}}\begin{bmatrix} 1 & \dfrac{t}{Y_{ri}} \\ Y_{ri}t & 1 \end{bmatrix}. \tag{10}$$

This ABCD matrix represents the series connection of a shunt short-circuited stub of characteristic admittance Y_r, a unit admittance 180^o phase shifter and a transmission line of characteristic admittance Y_{ri}. Thus the equivalent circuit of case 2 is as shown in Fig 7(a). Resonance is achieved at node r by capacitively loading port i' as shown in Fig. 7(b) and Fig. 8. This is a convenient form of realization because the lumped fringing capacitance at the bottom end of the inner line (port i') and the open-circuit end of the middle line (port r) may be independently controlled allowing independent tuning of the resonant frequency and the transmission zero location associated with each resonator.

The input impedance of circuit of Fig. 7(b) may be computed as

$$Z_{in}(j\omega) = j\frac{Z_r Z_{ri}(\omega C_r Z_{ri}\tan(a\omega) - 1)\tan(a\omega)}{Z_r \tan^2(a\omega) - Z_{ri} + \omega C_r Z_{ri}(Z_r + Z_{ri})\tan(a\omega)} \tag{11}$$

where

$$a = \frac{\theta_o}{\omega_o} \tag{12}$$

And

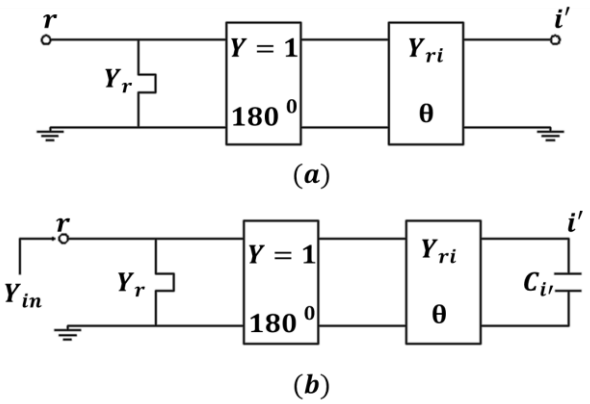

Fig. 7. Case 2 - Re-entrant resonator circuit realizing a transmission zero above passband (a) equivalent circuit (b) resonance circuit

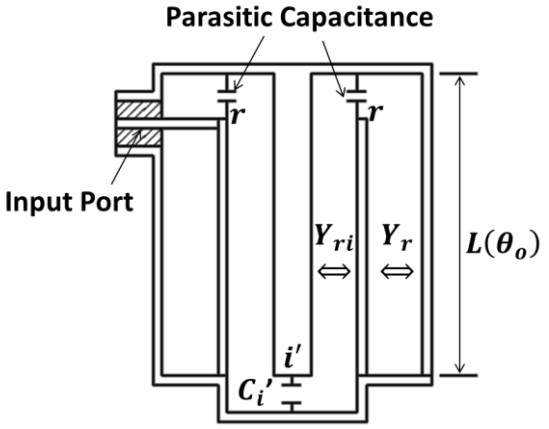

Fig. 8. Cross section of a physical realization of circuit of Fig. 7 (b)

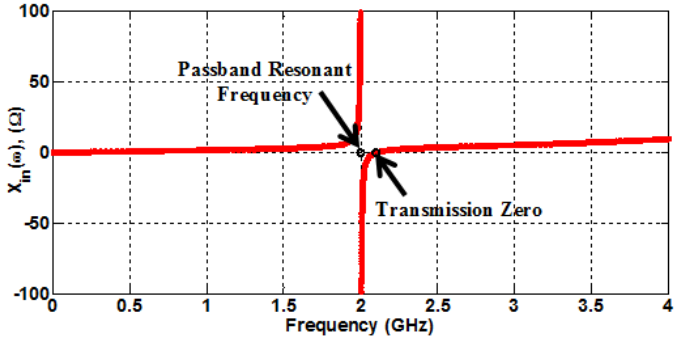

Fig. 9. Reactance function $X_{in}(\omega)$ plot corresponding to circuit of Fig. 7 (b)

$$C_r = \frac{1}{\omega_z Z_{ri}\, tan(a\omega_z)}$$

$$Z_r = \frac{Z_{ri}(1 - \omega_o C_r Z_{ri} \tan(a\omega))}{tan(a\omega_o)\,(tan(a\omega_o) + \omega_o C_r Z_{ri})} \tag{13}$$

Similarly, circuit element values are obtained for example if $f_o = 2\ GHz$, $f_z = 2.2\ GHz$, $\theta_o = \pi/6\ rad$, and $Z_{ri} = 77\ \Omega$, then using (12) - (13), $C_r = 1.45\ pF$ and $Z_r = 12.94\ \Omega$. The plot of the reactance function $X_{in}(\omega)$ of $Z_{in}(j\omega)$ against frequency is shown in Fig. 9 for the above example.

B. Re-entrant Resonator producing a transmission zero below the passband

A transmission zero below the passband may be achieved by terminating port r' and port i' of the re-entrant line in Fig. 2 with an open-circuit and short-circuit respectively. The equivalent circuit of the resulting two port network is found by reducing the four port admittance matrix of the re-entrant line to a two-port admittance matrix as was done for case 2 of section II (A). The equivalent circuit between port r and i may then be obtained directly from the 2-port admittance matrix or conversion into ABCD matrix as shown in Fig. 10(a). Capacitively loading port i produces the resonant circuit as shown in Fig. 10(b) and Fig. 11.

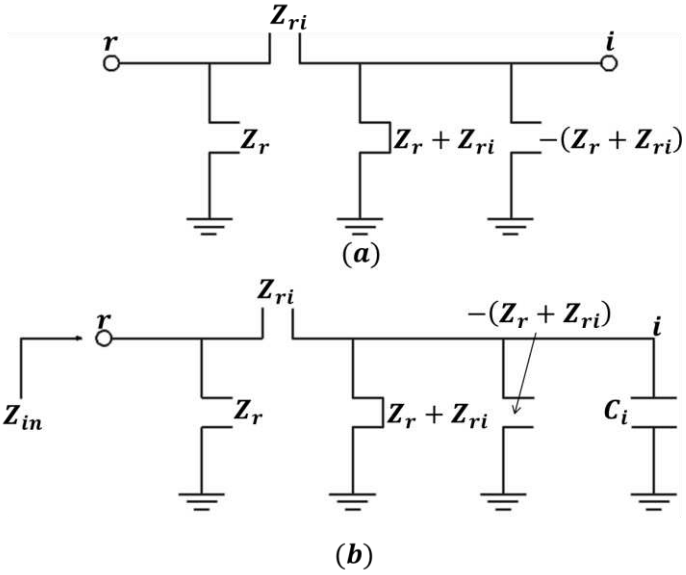

Fig. 10. Re-entrant resonator circuit that realizes transmission zero below the passband (a) equivalent circuit (b) resonance circuit

The input impedance of circuit of Fig. 10(b) may be computed as

$$Z_{in}(j\omega) = j\frac{Z_r Z_{ri} - Z_r{}^2 \tan^2(a\omega) - \omega Z_r Z_{ri} C_i (Z_r + Z_{ri}) \tan(a\omega)}{(Z_r + Z_{ri}) \tan(a\omega)\,(\omega C_i (Z_r + Z_{ri}) \tan(a\omega) - 1)} \tag{14}$$

where

$$a = \frac{\theta_o}{\omega_o} \tag{15}$$

and

$$Z_r = \frac{(\omega_o \tan(a\omega_o) - \omega_z \tan(a\omega_z))}{\omega_o \tan(a\omega_o)\, tan^2(a\omega_z)} Z_{ri}$$

$$C_i = \frac{1}{\omega_o (Z_r + Z_{ri}) \tan(a\omega_o)} \tag{16}$$

Circuit element values are obtained for example if $f_o = 2\ GHz$, $f_z = 1.95\ GHz$, $\theta_o = \pi/6\ rad$, and $Z_{ri} = 77\ \Omega$, then using (15) - (16), $Z_r = 13.32\ \Omega$ and $C_i = 1.53\ pF$. Finally, the plot of the reactance function $X_{in}(\omega)$ of $Z_{in}(j\omega)$ against frequency is shown in Fig. 12.

Though, it is theoretically possible to realize transmission zeros below the passband using the re-entrant structure of Fig.

11, its physical construction is impractical for real applications as it requires the suspension of the middle conductor. For this reason, design theory has only been fully developed for case 2 of section II (A) for re-entrant bandpass filters with transmission zeroes above the passband.

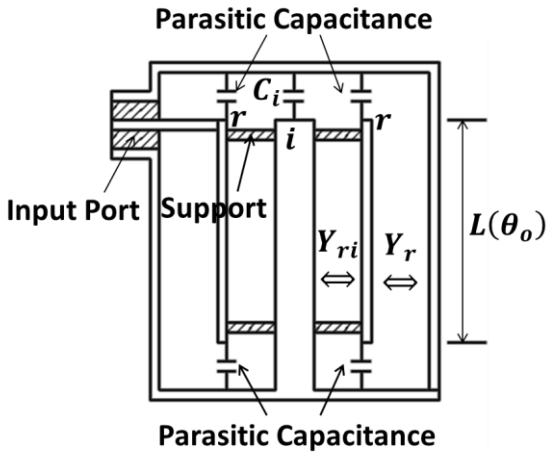

Fig. 11. Cross section of a physical realization of circuit of Fig. 10 (b)

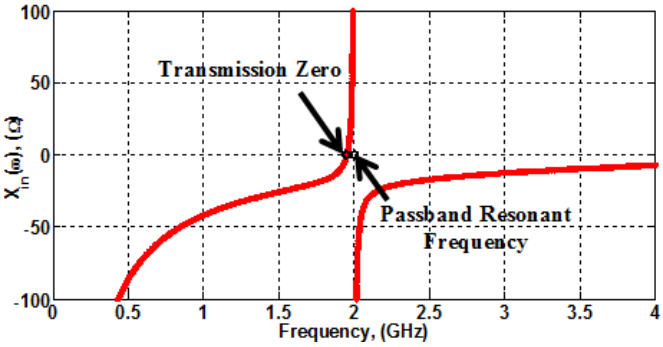

Fig. 12. Reactance function $X_{in}(\omega)$ plot corresponding to circuit of Fig. 10 (b)

III. Design Theory

Having obtained the equivalent circuit of a re-entrant resonator, design theory to obtain the re-entrant line element values for bandpass filter design is now derived.

A. Re-entrant Bandpass Filter Equivalent Circuit

The equivalent circuit of two coupled nodes in the re-entrant bandpass filter with case 2 resonators may easily be obtained from [5] by considering two middle transmission lines of the re-entrant resonators, short-circuited at one end and then superimposing the equivalent circuit towards the inner transmission lines at node r and $r+1$. This is synonymous to a combline bandpass filter except for the inner transmission lines. Therefore, the equivalent circuit of the N^{th} re-entrant bandpass filter is simply the interconnection of N re-entrant resonator circuits of Fig. 7 (b) in section II (A) by coupling series short-circuited stubs. Fig. 13 shows the equivalent circuit of the N^{th} degree re-entrant bandpass filter. Note that the 180^o phase shifters in Fig. 7 (b) may be ignored as they only account for the phase and have no effect on the magnitude response. Admittance inverters may be formed by adding shunt short-circuited stubs at r^{th} and $(r+1)^{th}$ nodes as in Fig. 14 where,

$$K_{r,r+1} = \frac{Y_{r,r+1}}{\tan(\theta)}. \tag{17}$$

The positive shunt short-circuited stub admittances in circuit of Fig. 14 are absorbed at the surrounding nodes leading to the final equivalent circuit as shown in Fig. 15 where,

$$\begin{aligned} Y_{11} &= Y_1 + Y_{12} \\ Y_{rr} &= Y_r + Y_{r-1,r} + Y_{r,r+1} \\ Y_{NN} &= Y_N + Y_{N-1,N} \end{aligned} \tag{18}$$

It is now left to derive the frequency transformation from a suitable lowpass prototype that preserves the frequency response so that the bandpass elements in (17) and (18) may be determined.

B. Lowpass Prototype

One suitable lowpass prototype is shown in Fig. 17 consisting of a shunt frequency invariant reactance (B_r) in parallel with a shunt series of an inductor $(1/b_r)$ with frequency invariant reactance $(-\omega_r/b_r)$ separated by frequency invariant admittance inverters $K'_{r-1,r}$ and $K'_{r,r+1}$. Techniques found in [6] coupled with some circuit transformations may be used to derive this lowpass prototype. For transmission zeros that are all at a single frequency ω_r rad/s, however, an asymmetric frequency transformation defined by

$$\omega \rightarrow \frac{1-\omega_r\omega}{\omega-\omega_r}, \tag{19}$$

may be used on an all-pole Chebyshev filter characteristic shown in Fig. 16 to produce the required lowpass elements as in Fig. 17. This transformation transforms all the transmission zeros at infinite to a single finite frequency ω_r rad/s in the lowpass domain. Thus the Chebyshev all-pole network of shunt capacitors C_r separated by admittance inverters $K'_{r,r+1}$ may be transformed to the required lowpass prototype as

$$Y'_{in}(j\omega) = j\omega C_r = j\left(\frac{1-\omega_r\omega}{\omega-\omega_r}\right)C_r. \tag{20}$$

which may be re-written as,

$$Y'_{in}(j\omega) = -j\omega_r C_r + \frac{C_r({\omega_r}^2-1)}{j\omega - j\omega_r} = jB_r + \frac{b_r}{s-j\omega_r}. \tag{21}$$

Where,

$$\begin{aligned} B_r &= -\omega_r C_r \\ b_r &= C_r({\omega_r}^2-1) \end{aligned} \tag{22}$$

The frequency invariant admittance inverters $K'_{r,r+1}$ between the nodes in the Chebyshev lowpass prototype remain unchanged by this transformation.

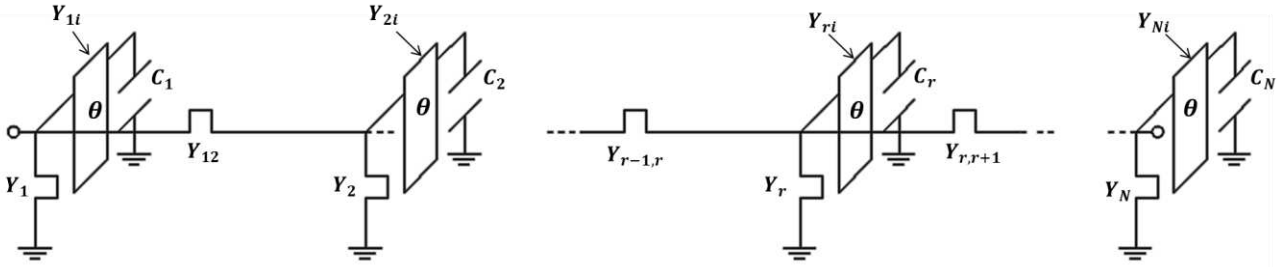

Fig. 13. Equivalent circuit of an N^{th} degree re-entrant bandpass filter

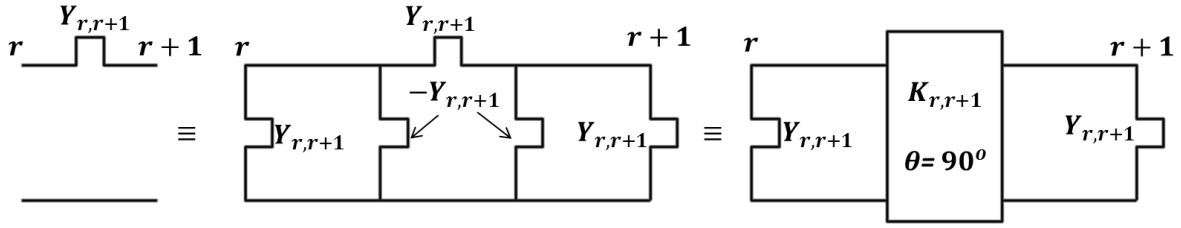

Fig. 14. Formation of admittance inverters between node r and $r+1$

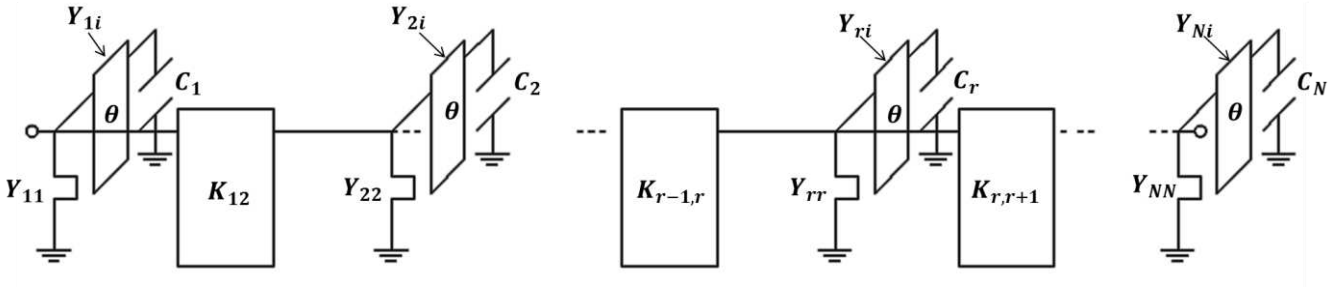

Fig. 15. Final equivalent circuit of an N^{th} degree re-entrant bandpass filter with admittance inverters

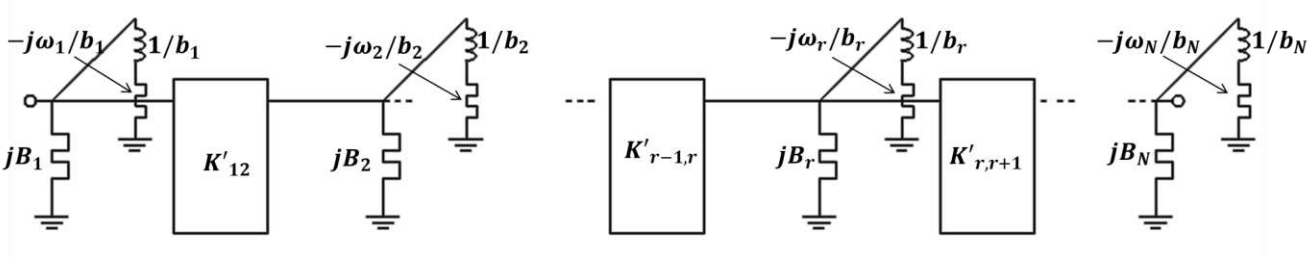

Fig. 16. N^{th} degree all-pole Chebyshev lowpass prototype filter with admittance inverters

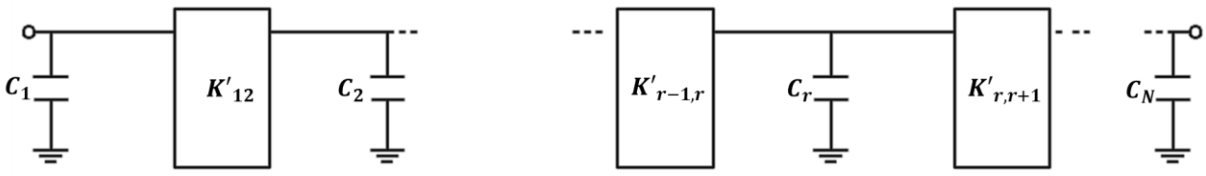

Fig. 17. N^{th} degree lowpass prototype used in the design of re-entrant bandpass filters

C. Frequency Transformation

In order to make the admittance inverters frequency invariant in the re-entrant bandpass equivalent circuit, the admittance of the entire network is scaled by $\tan(\theta)/\tan(\theta_o)$, where θ_o is the electrical length of the re-entrant resonator at the center frequency. The source and load admittances are also scaled by $\tan(\theta)/\tan(\theta_o)$ but the variations of $\tan(\theta)/\tan(\theta_o)$ is small for narrow bandwidth filters. Thus the

frequency invariant admittance inverters are mapped as

$$K_{r,r+1} = \frac{Y_{r,r+1}}{tan(\theta_o)} = K'_{r,r+1}. \quad (23)$$

Hence,

$$Y_{r,r+1} = K'_{r,r+1} tan(\theta_o). \quad (24)$$

Furthermore, the frequency variant admittance at r^{th} node of the re-entrant bandpass, (11), maps onto the admittance at r^{th} node of the lowpass filter, (20), as shown below.

$$\left(\frac{1-\omega_r\omega}{\omega-\omega_r}\right) C_r \Rightarrow \frac{\alpha_r - \alpha_r\beta_r\omega\tan(\theta) - \tan^2(\theta) - \beta_r\omega\tan(\theta)}{\gamma_r\tan(\theta_o) * [\beta_r\omega\tan(\theta) - 1]} \quad (25)$$

Where,

$$\alpha_r = \frac{Y_{rr}}{Y_{ri}}, \beta_r = \frac{C_r}{Y_{ri}} \text{ and } \gamma_r = \frac{1}{Y_{ri}} \quad (26)$$

Fig. 18 illustrates the frequency mapping defined using (25) above. The parameters α_r, β_r and γ_r may be determined by mapping the centre frequency, $\omega = 0$ and the two bandedge frequencies at $\omega = \pm 1$ of the lowpass prototype onto the centre frequency ω_o , lower cut-off frequency ω_1 and upper cut-off frequency ω_2 respectively of the re-entrant bandpass filter using (25) and solving the resulting non-linear equations for the variables α_r, β_r and γ_r at each node r. The re-entrant bandpass element values are then obtained as follows:

$$Y_{ri} = \frac{1}{\gamma_r}, Y_r = \frac{\alpha_r}{\gamma_r} \text{ and } C_r = \frac{\beta_r}{\gamma_r} \quad (27)$$

Finally the entire network nodal admittance matrix may be scaled at the nodes to yield realizable impedance values. The input and output connections are made by direct tap onto the first and last middle conductors. Redundant coupled lines at input and output may also be added if desired.

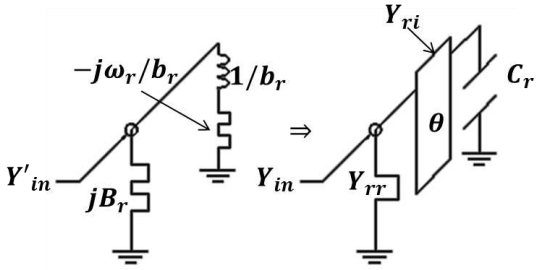

Fig. 18. Frequency mapping of the admittances at r^{th} node

D. Close-to-Band Transmission Zeroes

In this section, the limitation of the transmission zero locations is discussed with respect to the element realisations. For example for the transmission zero above the passband re-entrant structure of Fig. 8, consider a single resonator where the bandwidth is controlled by the input and output couplings, then using (13) of section II (A) for $f_o = 1\,GHz$ and $Z_{ri} = 77\,\Omega$, the ratio of Z_{ri}/Z_r and C_r were plotted against the transmission zero locations as depicted in Fig. 19. It is clear from Fig. 19 that the ratio Z_{ri}/Z_r increases as the transmission zero location gets closer to the upper passband edge. As the transmission zeros get very close to the passband, clearly Z_r becomes unrealizable small. Increasing θ_o from $\theta_o = 30^o$ in Fig. 19 (a) to $\theta_o = 45^o$ in Fig. 19 (b) increases the ratio Z_{ri}/Z_r while the capacitance loading C_r decreases. This means Z_r decreases for a fixed Z_{ri}. By using a different θ_o a similar analysis may be done to determine the location of the transmission zeros that will give realizable Z_r given Z_{ri}. For a given bandwidth and centre frequency, the closest transmission zero to the passband the structure can support would be determined by the realisability of Z_r for a fixed Z_{ri} by using an appropriate electrical length (θ_o). Thus the structure can realize transmission zeros as close as one passband bandwidth away from the passband edge. More specific design examples and impedance levels for the elements will be given later.

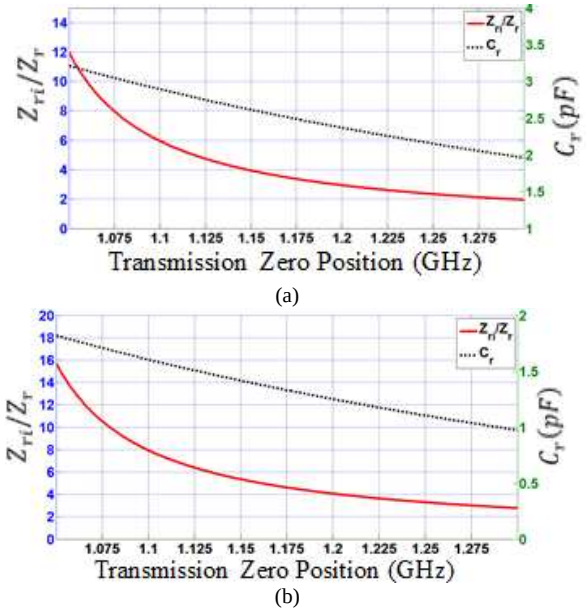

Fig. 19. (a) Element values vs transmission zero positions $f_o = 1$ GHz, and $\theta_o = 30^o$and $Z_{ri} = 77\ \Omega$ (b) Element values vs transmission zero positions $f_o = 1$ GHz, and $\theta_o = 45^o$and $Z_{ri} = 77\ \Omega$

E. Physical dimensions

With the element values known, calculation of the physical dimensions is fairly straight forward using established methods already used for combline and interdigital bandpass filters as explained in [7-8]. The inner transmission lines are realized as circular coaxial lines which are easy to machine. One end of the inner re-entrant line is fixed to the upper metallic wall (cover) by screwing it into the wall. Metallic discs may be fitted to the other end of the inner re-entrant line to achieve the required capacitive loading. The middle transmission lines may be realized with circular or rectangular rods. The ground spacing is chosen to achieve the given unloaded Quality factor, Q_u and that there is sufficient space for the inner re-entrant conductor.

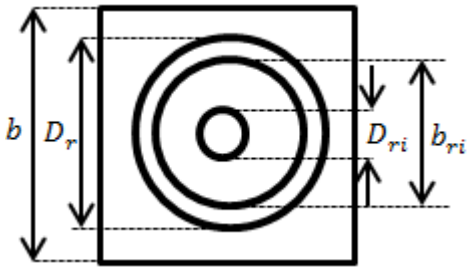

Fig. 20. Re-entrant resonator cross section corresponding to Fig. 8 structure of section II (A) case 2 with square outer conductor and circular middle and inner conductors and height H (not shown)

TABLE I Air-Filled Re-entrant Resonator With $b = 35\ mm, b_{ri} = 18\ mm, D_{ri} = 4.99\ mm, H = 25\ mm$				
Middle Conductor D_r (mm)	Resonant Frequency (GHz)	First Spurious (GHz)	Unloaded Q_u	Q_u per Volume (mm^{-3})
32.14	1.02	2.82	1805	0.055
24.43	1.01	2.76	2226	0.067
Air-Filled Coaxial Resonator With $b = 35\ mm, H = 25\ mm$				
Inner Conductor D_r (mm)	Resonant Frequency (GHz)	First Spurious (GHz)	Unloaded Q_u	Q_u per Volume (mm^{-3})
13.89	1.00	6.16	3386	0.111

It is quite obvious that the advantages of the re-entrant resonator of having close-to-band transmission zeros creating high stopband rejection and simple in-line structure do have tradeoffs. The theoretical spurious resonance is three times the center frequency for $\theta_o = 30^o$. However, because of the presence of the parasitic capacitance on one end of the middle conductor, the spurious resonances actually appear closer to the first passband. Furthermore, choosing relatively large ground spacing pushes these farther down in frequency. Table I shows the unloaded Q_u and spurious performance for a re-entrant resonator compared to the normal coaxial resonator of comparative size using HFSS assuming silver plated conductors. Following up from section III (D), it may be seen that for fixed inner conductor dimensions, the transmission zero is controlled by the middle conductor dimension, i.e. D_r as shown in Fig. 20. Therefore, for a fixed ground plane spacing (b) and as the position of the transmission zero gets closer to the passband, D_r increases. The middle conductor dimension in Table I corresponds to a transmission zero position at 1.075 GHz (32.14 mm) and 1.2 GHz (24.43 mm) respectively. It is clear from table I that the unloaded Q_u is lower in re-entrant resonator and further degrades for much closer-to-band transmission zeros above the passband.

The requirement to physically incorporate two conductors within the same physical structure and to improve the unloaded Q_u does mean that the re-entrant filter would require relatively large resonator size. However, in certain cellular applications where deep stopband rejections are required on the upper side of the passband, the re-entrant resonator bandpass filter would provide a good alternative solution.

IV. Design Example

A. Design Example I

A 5 pole reentrant bandpass filter with centre frequency at 1 GHz, 50 MHz bandwidth and 20 dB return loss was designed. The filter were designed with the following arbitrary located transmission zeros as:

$$\omega_r = [7.1616, 3.4, 3, 3.2, 4.44, 7.1404]\ rad/s$$

corresponding to microwave frequencies:

$$f_r = [1.147, 1.077, 1.068, 1.098, 1.147]\ GHz.$$

Firstly the elliptic lowpass with arbitrary transmission zeros was synthesised corresponding to the circuit of Fig. 17 above. The obtained element values are shown in table II below.

The bandpass element values are obtained by application of (24-27) and (18) as described in section III (C). The electrical length at the center frequency was chosen to be $\theta_o = 30^o$. After the bandpass frequency transformation and scaling so that the inner re-entrant lines are identical for all resonators (i.e. $Z_{ri} = 77\ \Omega$), the element values were determined as shown in table III in a $50\ \Omega$ system.

TABLE II: Elliptic Lowpass Filter Element Values		
B_r	b_r	K_{ij}'
−7.0647	48.8958	0.2192
−0.2262	0.6968	0.0440
−0.2158	0.5744	0.0331
−0.1693	0.7069	0.1658
−6.9901	48.6018	

TABLE III: Re-entrant Bandpass Filter Element Values $Z_{ri} = 77\ \Omega$			
Middle Conductors	Capacitors	Coupling admittances	Input and Output Coupling
$Z_1 = 27.5963\ \Omega$	$C_1 = 2.6265\ pF$	$Z_{12} = 53.9827\Omega$	$Z_{s1} = 50\ \Omega$
$Z_2 = 15.2545\ \Omega$	$C_2 = 3.0335\ pF$	$Z_{23} = 33.9059\Omega$	$Z_{7l} = 50\ \Omega$
$Z_3 = 12.8267\ \Omega$	$C_3 = 3.0868\ pF$	$Z_{34} = 43.6124\ \Omega$	
$Z_4 = 20.7958\ \Omega$	$C_4 = 2.9050\ pF$	$Z_{45} = 69.1771\ \Omega$	
$Z_5 = 25.1697\ \Omega$	$C_5 = 2.6271\ pF$		

The circuit simulation is shown in Fig. 21. All the element values shown are realisable with the middle conductors realised in rectangular coaxial profile, while the inner transmission lines are realised with circuilar coaxial and are identical. The input and output feed is implemented by means of a tap near the top of the first and last resonators. The close to band transmission zero at 1.068 GHz is created by the centre resonator as evidenced by the smallest characteristic impedance ($Z_4 = 12.8267\ \Omega$). This impedance may easily be scaled up if necessary. The outermost transmission zeros at 1.145 GHz are created by the the first and last resonators. Deep stopband rejection of about 120 dB is achieved around the transmission zeros positions.

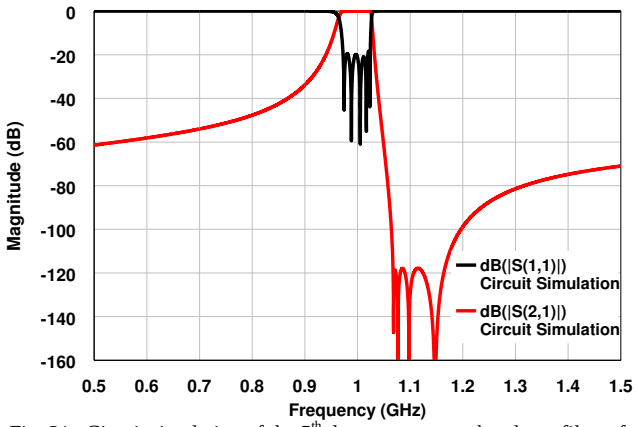

Fig. 21. Circuit simulation of the 5th degree re-entrant bandpass filter of example I

B. Design Example II

A 5 pole re-entrant bandpass filter with centre frequency at 1 GHz, 85 MHz bandwidth, 20 dB return loss and 1 dB maximum insertion loss across ripple bandwidth was designed. A lowpass filter was first designed with all the transmission zeroes placed at $\omega_r = 5.5\ rad/s$, corresponding to microwave frequency of $1.1466\ GHz$.

TABLE IV: Re-entrant Bandpass Filter Element Values		
Inner conductors	Middle Conductors	Coupling admittances
$Z_{ri} = 77.1598\ \Omega$ $C_r = 2.3658\ pF$	$Z_1 = Z_5 = 32.9867\Omega$ $Z_2 = Z_4 = 43.1568\ \Omega$ $Z_3 = 38.8326\ \Omega$	$Z_{12} = Z_{45} = 102.84\ \Omega$ $Z_{23} = Z_{34} = 139.98\ \Omega$

TABLE V: Filter Theoretical (Calculated) Physical Dimensions (mm)			
$D_{ri} = 1.97$	$b = 40$	$sw1 = 20$	$w1 = 12.88$
$D_r = 7.14$	$H = 25$	$s12 = 8$	$w2 = 11.14$
$t = 32.00$	$h = 4.2$	$s23 = 10.4$	$w3 = 12.52$

The Chebyshev lowpass filter with $20\ dB$ return loss was synthesized with elements values C_r and $K'_{r,r+1}$ obtained. Then (19) was used to obtain the element values of the lowpass prototype required for the design of the re-entrant bandpass filter. As in example I, the bandpass element values are obtained by application of (24-27) and (18) as described in section III (C). The electrical length at the center frequency was chosen to be $\theta_o = 30^o$. After the bandpass frequency transformation and scaling so that the inner re-entrant lines are identical for all resonators, the element values in a $50\ \Omega$ system were determined as shown in table IV. The circuit simulation is shown in Fig. 22 below.

TABLE VI: Filter Dimensions after Optimization (mm)			
$D_{ri} = 5.02$	$b = 40$	$sw1 = 20$	$w1 = 23.63$
$D_r = 17.88$	$H = 25$	$s12 = 7.8$	$w2 = 21.88$
$t = 32.00$	$h = 4.2$	$s23 = 10.4$	$w3 = 23.27$

The physical dimensions were determined as described in section III (E) and using [8] as shown in Table V. The ground spacing of 40 mm was used in the design. The physical structure was simulated using HFSS and optimized. Note as always [9], the theoretical design underestimate the actual bandwidth in combline filter design using [8]. The optimized physical dimensions are given in Table VI and depicted in Fig. 23 below. Note also that the inner conductor dimensions were not optimized but were proportionally increased so that the characteristic impedance ($Z_{ri} = 77.1598\ \Omega$) is maintained. The overall filter cavity dimensions were 40 mm wide, 190.69 mm in length and 29.2 mm in height. The filter was fabricated using Aluminium with the above physical dimensions.

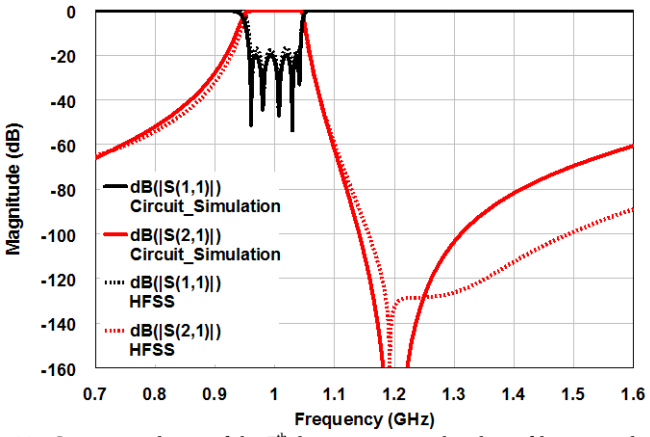

Fig. 22. Circuit simulation of the 5th degree re-entrant bandpass filter example II vs HFSS simulation

V. Results

Fig. 24 shows the comparison between the measured frequency response and HFSS (lossless) simulation whereas Fig. 25 shows the same simulation on a broader frequency scale. In the re-entrant bandpass filter, the coupling admittances are considerably smaller than in normal combline bandpass filter of comparable bandwidths. This means that the inter-resonator spacings are relatively smaller. Thus significant fringing capacitance between non-adjacent resonators do exist and potentially leading the method in [8] for obtaining physical dimensions inaccurate. Thus the bandwidth is considerably broader with initial values obtained using [8]. However, this bandwidth change also occurs in conventional combline filters. As noted in [9], the problem may be solved by utilizing full EM simulators or alternatively using bandwidth correction factors may be less time consuming. Further adjustment may be achieved by mechanical tuning using tuning screws in the fabricated filter. The filter fabricated hardware is shown in Fig. 26 below.

A. Selectivity

The re-entrant bandpass can realize a maximum of N transmission zeroes equivalent to the filter order making it relatively very selective filter. Additionally, the design presented above provides for flexibility in position of the transmission zeroes. The transmission zeros above the passband may be located as near as one passband away from

the bandedge. The fundamental limit to the placement of transmission zeroes is that as the transmission zeroes become much closer to the passband edge the impedance levels are unrealizably small or large.

B. Symmetrical Design

The re-entrant bandpass may be realized using physically symmetrical or asymmetrical in-line structures depending on transmission zero placements. Physically symmetrical design may be achieved by placing transmission zeroes so that each node from the two opposite ends have the same transmission zero. For example for a 5 pole and 5 transmission zeroes filter, the lowpass transmission zero distribution may be chosen as $\omega = 2,3,4,3,2\ rad/s$ or $\omega = 5,10,10,10,5\ rad/s$ - all produce physically symmetrical designs. Alternatively, all the transmission zeroes may be placed at a single frequency. Although this does not improve the overall stopband rejection, it does simplify the synthesis, design and tuning of the filter. Physically symmetrical structures make for easy of tuning the filter after fabrication and as well as cut down design time when optimizing using time consuming EM software such as HFSS.

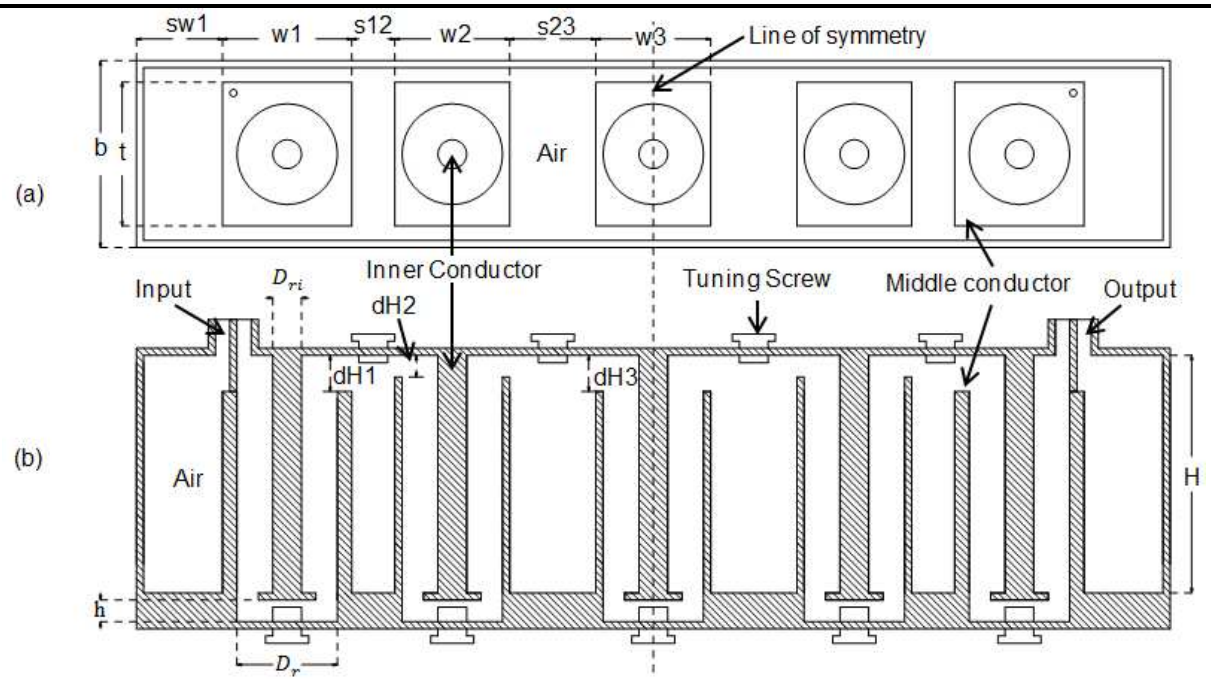

Fig. 23. Diagram showing the layout of the re-entrant resonators in the design example of part IV: (a) Top view (b) Cross section of side view - dimensions shown are as given in table IV.

C. Tunability

The filter tuning is achieved by screws that control the lumped capacitance on the inner transmission lines of the re-entrant resonators. The tuning of the lumped capacitance controls both the resonant frequency and the transmission zero location. Aditional tuning screws may be inserted on top of the filter to control the resonance frequency by slight adjustment of the capacitance at the open-circuited end of the middle conductors. Coupling screws may also be inserted between the nodes to control the couplings. The fabricated filter was easy to tune as all the inner conductors' dimensions were identical requiring identical turns in the tuning screws.

D. Compact In-Line Filter Structure

In the re-entrant bandpass filter design presented above, the resonator lengths at the center frequency may be made considerably short e.g. $\theta_o = 30^o$. The re-entrant resonators also require strong couplings for very close-to-band transmission zeroes resulting in smaller inter-resonator spacing. Thus the filter may considerably be reduced in size. However, the requirement to have an inner conductor inside the middle conductor does limit the choice of the ground spacing. In addition, the in-line filter topology makes an ideal realization for base station filters.

The highly selective re-entrant resonators may also be mixed with normal combline resonators with much wider spurious free frequency window to exploit the better of 'both worlds.' Furthermore, the re-entrant bandpass filter is easy to fabricate, like in combline bandpass filters, as all the middle transmission lines are fixed and short-circuited at one end whereas the inner transmission lines may be fabricated separately and fixed to the filter cover by screwing them into the cover as depicted in the fabricated filter photos in Fig. 26 above. The tuning screws located on the same side of the filter bottom wall make for easy of tuning.

VI. Conclusions

The design of a highly selective re-entrant microwave bandpass filter with arbitrarily placed transmission zeros above the passband has been demonstrated. A five pole re-entrant bandpass filter was designed and fabricated. The

measured results showed good agreement with established theories. The filter offers significant advantages over conventional design when very high stopband attenuation is required.

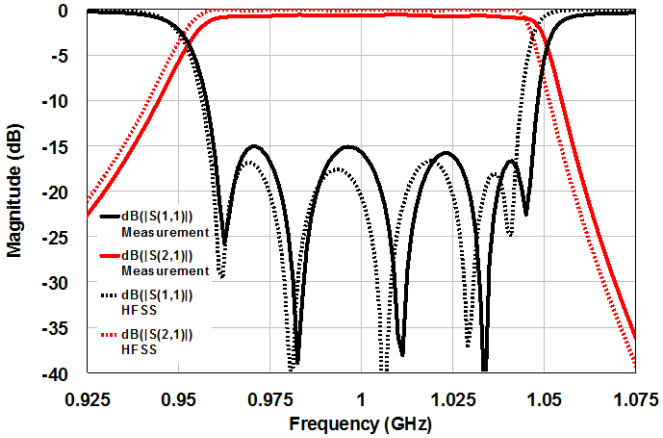

Fig. 24. Measured vs HFSS frequency response of the fabricated re-entrant bandpass prototype.

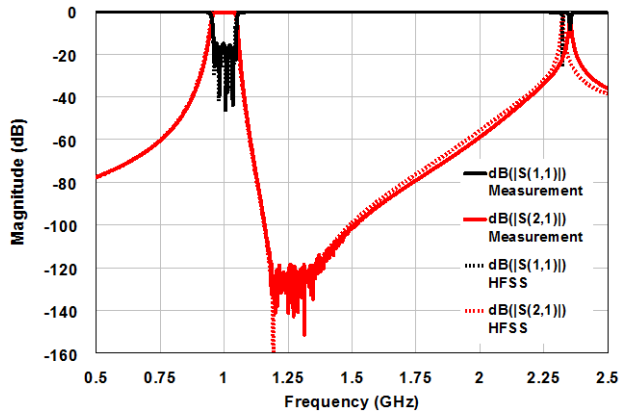

Fig. 25. Measured versus HFSS simulation of the fabricated re-entrant bandpass filter

(a)

(b)

Fig. 26. Photo showing a fabricated re-entrant bandpass filter (a) filter with top cover removed (b) assembled filter with input and output connectors

REFERENCES

[1] R. J. Cameron, C. M. Kudsia, and R.R. Mansour, "Microwave filters for communication systems: fundamentals, design, and applications," Vol. 1. Wiley-Interscience, 2007.

[2] S. B. Cohn, "The re-entrant cross section and wide-band 3-dB hybrid couplers," IEEE Trans. Microw. Theory Techn., vol. 11, no. 4, pp. 254-258, 1963

[3] M. C. Horton, R. J. Wenzel, "The digital Elliptic Filter – A compact sharp-cutoff design for wide bandstop or bandpasss requirements," IEEE Trans. Microw. Theory Techn., vol. 15, no. 5, pp. 307-314, 1967.

[4] J. A. Ruiz-Cruz, M. M. Fahmi, and R. R. Mansour, "Triple-conductor Combline resonators for dual-band filters with enhanced guard-band selectivity," IEEE Trans. Microw. Theory Techn., vol. 60, no. 12, pp. 3969-3979, 2012.

[5] R. Sato, and E. G. Cristal, "Simplified analysis of coupled transmission-line networks," IEEE Trans. Microw. Theory Techn., vol. 18, no. 3, pp. 122-131, 1970.

[6] I. C. Hunter, "Theory and design of microwave filters," The institute of electrical engineers, London, 2001

[7] G. MATTHAI, L. Young, and E. JONES, "Microwave filters, impedance matching networks and coupled structure," McGraw-Hill Company, 1964.

[8] M. A. R. Gunston, "Microwave transmission-line impedance data," Van Nostrand Reinhold, London, 1972.

[9] A. Abramowicz, "Modelling of Wide Band Combline and Interdigital Filters," Society for Microwave Theory and Technique, Microwave Review, vol. 16, no. 1, pp. 15-22, 2010.

Evaristo Musonda (GSM'13) received the B.Eng degree (with distinction) from The University of Zambia, Lusaka, Zambia, in 2007, the M.Sc. degree in communication engineering (with distinction) from The University of Leeds, Leeds, U.K., in 2012, and is currently working toward the Ph.D. degree at The University of Leeds. In early 2008 he joined Necor Zambia Limited, an ICT company, before joining the country's largest mobile telecommunication services provider, Airtel Zambia, in June 2008, where he was involved in core network planning, optimization, and support roles for three years. His research interests are microwave filters and network synthesis.

Ian Hunter (M'82–SM'94–F'07) received the B.Sc. degree (honors, first class) and Ph.D. degree from Leeds University, Leeds, U.K., in 1978 and 1981, respectively. Early in his career, he was with Aercom, Sunnyvale, CA, USA, and KW Engineering, San Diego, CA, USA, and Filtronic, Shipley, U.K., where he was involved with the development of broadband microwave filters for electronic warfare (EW) applications. From 1995 to 2001, he was with Filtronic Comtek, where he was involved with advanced filters for cellular radio. He currently holds the Royal Academy of Engineering/Radio Design Ltd. Research Chair in Microwave Signal Processing with the School of Electronic and Electrical Engineering, The University of Leeds, Leeds, U.K. He currently leads a team involved with the research of new microwave filters for mobile communications systems. He authored Theory and Design of Microwave Filters (IEE, 2001). Prof. Hunter is a Fellow of the IET and the U.K. Royal Academy of Engineering. He was general chair of 2011 European Microwave Week, Manchester, U.K. He will chair the 2016 European Microwave Conference, London, U.K.